DOI:
10.1021/acsomega.7b00131

Document Version
Publisher's PDF, also known as Version of record

ACS OMEGA

Article

http://pubs.acs.org/journal/acsodf

Computational Study Reveals the Molecular Mechanism of the Interaction between the Efflux Inhibitor PAβN and the AdeB Transporter from *Acinetobacter baumannii*

Shirin Jamshidi,[†] J. Mark Sutton,[‡] and Khondaker Miraz Rahman*[,†]

[†]Institute of Pharmaceutical Science, King's College London, London SE1 1DB, U.K.

[‡]National Infection Service, Public Health England, Porton Down, Salisbury, Wiltshire SP4 0JG, U.K.

Supporting Information

ABSTRACT: Phenylalanine-arginine β-naphthylamide (PAβN) is a broad-spectrum efflux pump inhibitor that has shown to potentiate the activity of antibiotics in Gram-negative bacteria. AdeB is a part of the AdeABC tripartite pump that plays a pivotal role in conferring efflux-mediated resistance in *Acinetobacter baumannii*. To understand the molecular mechanism of efflux pump inhibition by PAβN, we investigated the interaction of PAβN with AdeB using different computational methods. We observed that PAβN does not have specific binding interactions with the proximal binding site and interacts strongly with the distal binding pocket. The Phe loop located between the proximal and distal binding pockets plays a key role in the PAβN-mediated inhibition and acts as a gate between the binding pockets. Molecular dynamics simulations suggested that PAβN behaved like a climber as we observed switching of the interaction energies between the ligand and the key Phe residues of the binding site during the course of the simulation. PAβN uses the hydrophobic microenvironment formed by Phe residues in the distal binding pocket to keep the binding monomer in the binding conformation. The simulation data suggests that this binding event should result in the inhibition of the peristaltic mechanism and prevent the exporter from extruding any other substrates leading to the inhibition of the tripartite pump.

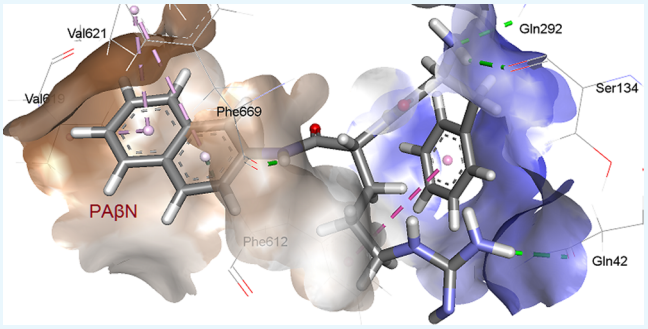

1. INTRODUCTION

Multidrug-resistant (MDR) bacteria have emerged as a major concern for public health, and there are particular concerns about the emergence of a number of Gram-negative pathogens, for which there are dwindling treatment options and few compounds are in development. These pathogens are characterized by the ability to rapidly develop and acquire resistance mechanisms in response to exposure to different antimicrobial agents. A key part of the armory of these pathogens is a series of efflux pumps, which effectively exclude or reduce the intracellular concentration of a large number of antibiotics and other compounds, making the pathogens significantly more resistant. These efflux pumps are a topic of considerable interest, both from the perspective of understanding efflux pump function and also as targets for novel adjunct therapies.

Resistance-nodulation-division (RND) multidrug efflux pumps are tripartite systems, situated in the three-layer (outer membrane, periplasmic space, and inner membrane) envelope of Gram-negative bacteria,[1] consisting of an outer membrane protein (OMP) or channel such as AdeC, TolC, or OprM; a fusion or accessory protein such as AdeA, AcrA, or MexA, which is located in the periplasmic space; and an inner membrane protein or transporter such as AdeB, AcrB, or MexB, which is located in the bacterial inner membrane.[2,3] Each of the three components of tripartite efflux pumps assembles as a homotrimer.[4−6]

The molecular structure of the inner membrane protein is composed of three regions: (i) periplasmic regions, including porter and docking domains (PN1, PN2, and DN) in its N-terminal and also porter and docking domains (PC1, PC2, and DC) in the C-terminal; (ii) pore regions; and (iii) transmembrane (TM) regions[4−6] (Figure 1). Four subdomains of PN1, PN2, PC1, and PC2 pack to form two proximal and distal substrate-binding pockets, which are separated by a switch glycine-rich loop, a part of PC1 with a Phe residue at the tip, namely, a G-loop or a Phe loop. The Phe loop controls the access of substrates to the distal pocket by forming a boundary between the proximal and distal binding pockets.[7] Under the Phe loop, there is a narrow channel that connects the proximal and distal pockets to each other. The pockets are enriched in aromatic, polar, and charged amino acid residues that form favorable interactions with the transported substrates. The

Received: February 6, 2017
Accepted: June 7, 2017
Published: June 28, 2017

DOI: 10.1021/acsomega.7b00131
ACS Omega 2017, 2, 3002−3016

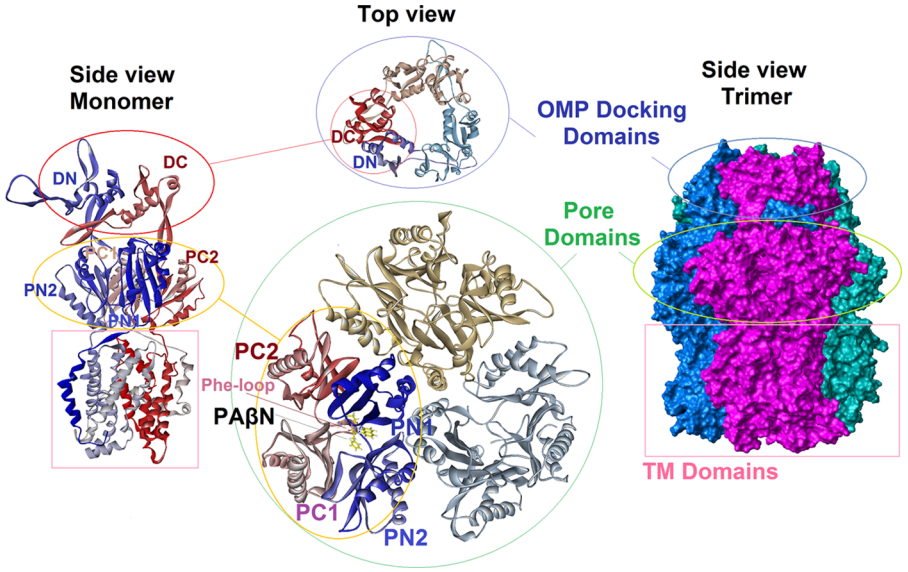

Figure 1. Proposed model structure of the AdeB efflux pump transporter from *Acinetobacter baumannii*. It represents the structure that was obtained after carrying out homology modeling, minimization, and equilibration. The full-space complete homotrimer structure of AdeB has been shown on the right side of the picture, and each subunit has been represented by different colors. The side view of the binding conformer has been shown on the left side of the picture. In addition, two top views of the docking (D) and pore (P) domains have been represented in the middle of the picture. The DC (C-terminal) and DN (N-terminal) subdomains of the docking section have been indicated by the top view in the top middle panel, and the PN1, PN2, PC1, and PC2 subdomains of the pore section have been indicated in the bottom middle picture with a 2 times magnification over the others. PAβN has been shown in the binding domain.

proximal and distal pockets show substrate preferences and can associate with different antibiotics including β-lactams.[8−10]

The monomers of the inner membrane protein can adopt three different states: access (loose), binding (tight), and extrude (release) to provide essential dynamics for the efflux.[4,9,11] Structures with bound drugs revealed two discrete multisite binding pockets separated by a switch loop, with the distal pocket in the binding (tight) state and the proximal pocket in the access (loose) state.[8,9]

Acinetobacter baumannii is a Gram-negative bacillus that causes numerous healthcare-associated infections worldwide, with a propensity for nosocomial transmission.[12] Reports have demonstrated the involvement of both intrinsic and acquired resistance determinants, as well as efflux pumps, in conferring multidrug resistance.[13] Several efflux pumps were identified and shown to be associated with multidrug efflux prior to the sequencing of the *A. baumannii* genome;[3−5] for example, efflux pumps adeABC, abeM, adeDE, and adeXY have been identified in *A. baumannii* through genetic analysis.[4,7,8,14] The overexpression of the adeABC pumps has been experimentally associated with the multidrug resistance phenotype in clinical isolates of *A. baumannii*.[9−11] In contrast, other transporter components such as adeIJK, adeFGH, and adeT were identified initially through genome analysis[12] and have only recently been shown to play a role in either intrinsic (adeIJK) or inducible drug resistance (adeFGH).[15]

Efflux pump system AdeABC was identified in a MDR *A. baumannii* strain in 2001.[1] In *A. baumannii*, AdeB is the multidrug transporter protein, AdeA is the membrane fusion protein, and AdeC is the OMP.[1] The efflux transporter (AdeB), as an inner membrane protein of tripartite efflux pumps like AcrD,[16] captures its substrates either from within the phospholipid bilayer of the inner membrane or from the cytoplasm and then transports them into the extracellular medium via the OMP (AdeC). Periplasmic protein AdeA mediates the cooperation between the AdeB and AdeC components. Drug transport by AdeB is driven by the TM electrochemical gradient of protons. As a member of the RND family, AdeABC efflux pumps are proton antiporters and exchange H+ ions for drugs.[17,18] The overexpression of this system plays a pivotal role in efflux-mediated resistance in clinical isolates[19,20] and reduces the antimicrobial efficacy of a broad spectrum of antimicrobials including aminoglycosides, tetracyclines, erythromycin, chloramphenicol (CHL), trimethoprim, fluoroquinolones, some β-lactams,[1,21−23] and tigecycline.[24,25]

Phenylalanyl arginyl β-naphthylamide (PAβN) (Figure 2), one of the best-studied efflux pump inhibitors (EPIs), is a widely used EPI that has been reported as a substrate for the MexAB−OprM pumps[26] and AcrAB-TolC that follows a sigmoidal kinetics[27] and is also shown to inhibit efflux of antibiotics[24,28] and biocides[29,30] in *A. baumannii*. PAβN has been studied in a wide range of Gram-negative bacteria, including *A. baumannii*, *Enterobacter aerogenes*, *Klebsiella pneumoniae*, *Salmonella enterica*, *Pseudomonas aeruginosa*, and *Campylobacter jejuni*,[26,31−34] and has shown to potentiate the activity of different antibiotics through its effect on a wide range of efflux pumps. Mechanistically, PAβN acts as a competitive inhibitor and prevents efflux of the antibiotics by binding with the substrate-binding pocket of the efflux pumps, which leads to potentiation of their activities.[35−39] Alternatively, because of a close location of the binding site, EPI binding may also generate steric hindrance, impairing antibiotic binding at its affinity site. PAβN has shown to inhibit AcrAB-TolC in *K. pneumoniae*, *Escherichia coli*, *Salmonella typhimurium*, and *E. aerogenes*[31,33,39,40] and multiple homologous systems including AdeFGH and AdeABC in *A. baumannii*[41,42] and CmeABC in *C. jejuni* and *Campylobacter coli*.[43,44]

Agents that inhibit the tripartite efflux pump systems can play a key role in reviving antibiotics to which bacteria have become

DOI: 10.1021/acsomega.7b00131
ACS Omega 2017, 2, 3002−3016

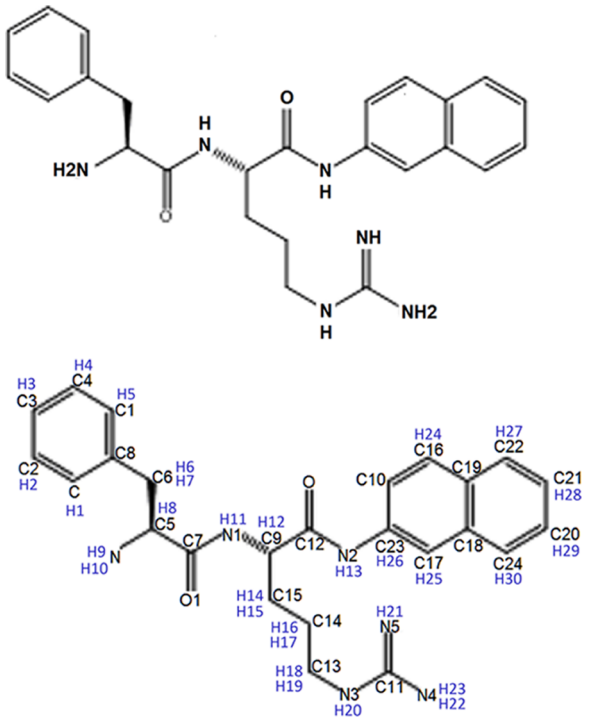

Figure 2. Structure (top) and atomtype (bottom) of phenylalanine-arginine β-naphthylamide (PAβN).

resistant.[18,45−50] Understanding how the transport process operates within the tripartite systems requires information on the organization and interaction of the subunits within a full tripartite assembly. Reconstituting tripartite assemblies for experimental structural elucidation has been a technical challenge, and simply mixing the components together does not yield the assembled complexes in sufficient yield or purity to enable analysis.[51] With the help of the available structural data, computational tools can be used to generate reliable models of these tripartite pumps and molecular dynamics (MD) simulations can provide detailed atomic-level information between EPIs and tripartite systems and help the researchers to understand the molecular mechanism of EPIs. This information is essential for designing new classes of EPIs with a better target affinity and desired EPI activity for clinical development.

In this study, for the first time, the interaction of PAβN with the binding monomer of *A. baumannii* AdeB homotrimer has been studied computationally. The data on the direct inhibition of AdeABC by PAβN appear to be contradictory. A number of studies have shown a clear effect of deletions in the components of the AdeABC pump, giving rise to a >4-fold increase in susceptibility to antibiotics such as GEN, ciprofloxacin (CIP), and tigecycline (e.g., Richmond's work),[52] but the studies have not been able to replicate this effect using PAβN (ref 41 and Sutton et al., unpublished) with only a very limited reduction in gentamicin (GEN) susceptibility observed in some cases. Conversely, PAβN does have a clear effect on the susceptibility to rifampicin and clarithromycin in *A. baumannii*, but the minimum inhibitory concentration of these antibiotics is apparently unaffected by knockout mutants or transposon insertions in *adeABC* (Sutton et al., unpublished).

Although molecular interaction of PAβN or other broad-spectrum EPIs with AdeB has not been studied to date, Vargiu and Nikaido[7] studied AcrB from *E. coli*, which is a similar efflux pump to AdeB by MD. A sequence alignment study reveals considerable differences (overall sequence identity 50.36%) between the positions of the critical amino residues (Figure S1 and Table S1) within the binding sites of the two pumps. Therefore, the interaction of EPIs with the binding sites of these transporters can vary, which in turn can affect the ability of these inhibitors to potentially block the pump. In addition to AdeB, there are other efflux pumps that also contribute to the MDR phenotype in *A. baumannii*; there is clear evidence that AdeB, as part of the AdeABC tripartite pump, is one of the most important systems. This is in terms of both the range of antibiotic classes that are potential substrates (e.g., mediating clinical resistance to all aminoglycosides][15] and the distribution of the efflux pump in MDR clinical isolates; prevalence approaches 100% in many clinically important lineages.[53−55] AdeB is a clinically important representative of the RND family of multidrug transporters in *A. baumannii*, and as such, the molecular mechanism of interaction of this pump with PAβN will provide useful new information to understand the substrate specificity of EPIs and balance the seemingly contradictory results seen for PAβN inhibition in *A. baumannii*. This information could then be used to design improved compounds that alone or in combination with antibiotics can block these MDR exporters and potentially sensitize resistant pathogens.

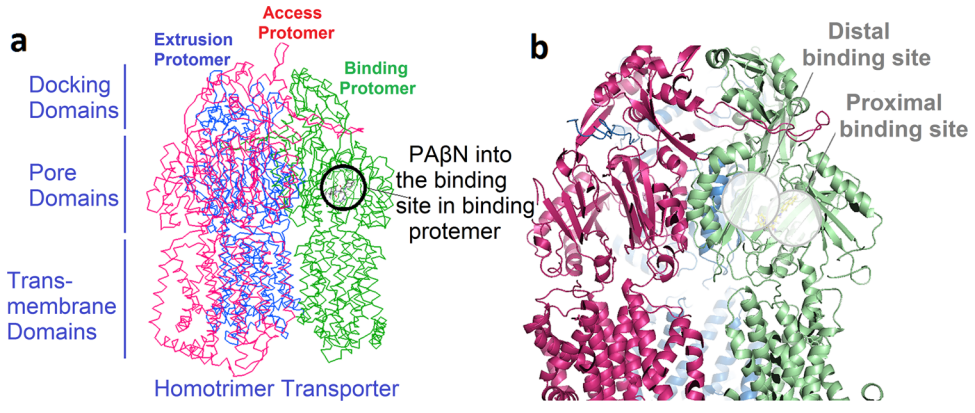

Figure 3. (a) Homotrimer of AdeB in complex with PAβN. Each monomer of the trimer has been shown in a different color; the best binding site in the binding monomer determined by Smina molecular docking somewhere close to the distal pocket that has been represented by a black circle. (b) PAβN in the multibinding sites within the binding protomer of the AdeB transporter.

DOI: 10.1021/acsomega.7b00131
ACS Omega 2017, 2, 3002−3016

Table 1. Interactions between AdeB's Key Residues and PAβN after GOLD Molecular Docking[a]

AdeB−PAβN atoms	distance	category	type
PAβN:N3:H−GLU665:OE2	2.2	hydrogen bond; electrostatic	salt bridge; attractive charge
THR668:OG1−PAβN:O1:H	2.7	hydrogen bond	conventional hydrogen bond
PAβN:N:H−SER134:OG	2.6	hydrogen bond	conventional hydrogen bond
PAβN:N:H−SER134:O	1.7	hydrogen bond	conventional hydrogen bond
PAβN:N:H−SER134:OG	2.9	hydrogen bond	conventional hydrogen bond
PAβN:N2:H−GLU665:OE2	2.0	hydrogen bond	conventional hydrogen bond
PAβN:N5:H−GLN42:OE1	2.2	hydrogen bond	conventional hydrogen bond
PAβN:N4:H−GLU665:OE1	2.8	hydrogen bond	conventional hydrogen bond
PAβN:N4:H−GLU665:OE2	2.9	hydrogen bond	conventional hydrogen bond
PAβN:C9:H−THR668:OG1	3.0	hydrogen bond	carbon hydrogen bond
ILE853:CD1−PAβN	3.6	hydrophobic	$\pi-\sigma$
PHE612−PAβN	3.8	hydrophobic	$\pi-\pi$ stacked
PHE612−PAβN	3.7	hydrophobic	$\pi-\pi$ stacked
PHE669−PAβN	4.2	hydrophobic	$\pi-\pi$ stacked
PAβN−MET570	5.0	hydrophobic	π-alkyl

[a]The distance cutoff and neighbor distance criterion were set to 5 and 4 Å, respectively. Proton donor−acceptor distance was considered for the H-bonds.

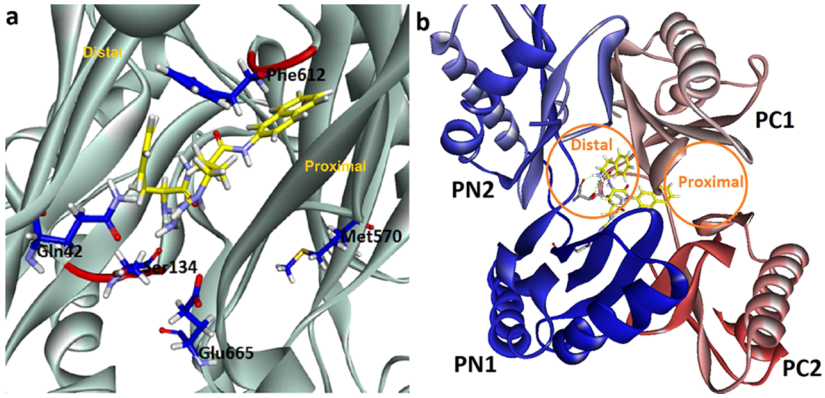

Figure 4. (a) PAβN located at the gate of the distal binding pocket in the intermolecular channel of the multibinding site between the Phe612 and Ser134 loops. The residues in stick presentation show the area of the binding site. (b) Top view of the multibinding site including PAβN in the binding protomer of the AdeB homotrimer transporter.

2. RESULTS AND DISCUSSION

2.1. Binding Site. According to the Smina molecular docking results, the location for binding of PAβN to the protein structure was identified in the multisite binding pocket within the binding protomer of the transporter (Figure 3). The docked complex of PAβN−AdeB was comparable to the previous structures determined for ligand-bound AcrB by Nakashima et al.[8] Only one PAβN was bound to the binding monomer of the homotrimer, and it was bound only to the multibinding site. Also, other favorable docked poses showed that PAβN could bind to the access monomer of the AdeB homotrimer, which suggests that PAβN could be forced to pass through the path, during the dynamic of the efflux process, by a transient conformational change from the access form to the binding form and PAβN would move to the gate of the distal pocket in the binding state. There were strong hydrophobic interactions between PAβN and Phe612 of AdeB that is located at the tip of the hairpin-like loop and forms a partition between the proximal and distal binding pockets at the top of the channel between the two pockets.

PAβN was found to bind to the narrow channel under Phe loop and partly in the distal binding site of AdeB after molecular docking (Figure 3b). The energy of binding, which corresponds to the affinity of the first pose (the best pose), obtained by the molecular docking of PAβN to the AdeB transporter showed that PAβN could associate to the multisite binding pocket with favorable affinity. Molecular modeling studies provided insight into the possible reason why PAβN could increase the susceptibility of certain antibiotics while has little effect against other antibiotics. To explore this further, we selected four antibiotics GEN, CHL, CIP, and levofloxacin (LEV) that are known substrates of AdeB. PAβN has shown to potentiate the activity of LEV in *P. aeruginosa* but has little effect on other three antibiotics. A blind molecular docking study was carried out to compare the binding site of these four antibiotics with that of PAβN. The best pose of GEN binds to the proximal binding pocket of the access protomer with an affinity of −9.6 kcal/mol, whereas the best poses of CIP and CHL bind to the extrude tunnel of the extrude protomer with affinities of −8.8 and −7.9 kcal/mol, respectively, whereas the best poses of PAβN and LEV bind to the distal pocket of the binding protomer with affinities of −9.3 and −7.7 kcal/mol respectively. This is consistent with the observation of Takatsuka et al.,[56] who showed that, by molecular docking in AcrB, PAβN predominantly binds to the hydrophobic groove (distal binding site), whereas CHL binds to the proximal binding pocket and is pumped out. Their docking study also showed that LEV seems to bind, at least predominantly, with its

DOI: 10.1021/acsomega.7b00131
ACS Omega 2017, 2, 3002−3016

Table 2. Interaction Energy between Different Phe Residues of the Phe-Cluster and PAβN in the AdeB−PAβN Complex during MD Simulation[a]

time (ns)	0	5	10	15	20	25	30	35	40	45	50
Phe residue and energy (kJ/mol)	Phe136	Phe136	Phe136	Phe136	Phe136	Phe136	Phe136	Phe136	Phe136	Phe136	Phe136
	−7.34	−5.13	−2.348	−0.78	−1.75	−1.19	−1.78	−1.78	−2.83	−3.2	−2.40
	Phe612	**Phe612**	**Phe612**	Phe573	**Phe612**	Phe573	Phe573	Phe573	Phe573	Phe573	Phe573
	−31.67	**−18.89**	**−26.52**	−0.86	**−26.06**	−0.32	−0.37	−0.37	−0.43	−0.38	−0.56
	Phe 623	Phe669	Phe669	**Phe612**	Phe669	**Phe612**	**Phe612**	**Phe612**	**Phe612**	**Phe612**	**Phe612**
	−2.57	−21.34	−21.48	**−31.14**	−19.19	**−21.73**	**−27.86**	**−27.86**	**−34.62**	**−32.63**	**−27.75**
	Phe669			Phe669		Phe669	Phe669	Phe669	Phe669	Phe669	Phe669
	−17.52			−19.97		−17.18	−18.72	−18.72	−21.45	−16.95	−13.56
	Phe 672										
	−0.98										

[a]The most favorable energy in each snapshot has been represented in bold font format that belongs to Phe12.

hydrophobic group bound to the upper groove of the binding site and with its hydrophilic group often exposed in the very wide substrate tunnel, which is in good agreement with the LEV orientation observed in the distal binding site of AdeB in the current study, which has been shown in Figure S2. In another study, Lomovskaya et al.[26] experimentally showed that although PAβN inhibits the LEV efflux by MexB in *S. aureus* and increases the susceptibility to this antibiotic, it was surprisingly much less effective in inhibiting the efflux of ethidium and carbenicillin. Also, GEN, which is not a substrate of MexB, was not affected by PAβN. The results of the current study also suggest that GEN, CHL, and CIP interact less favorably with the distal binding pocket and the addition of PAβN does not affect the ability of the pump to extrude these antibiotics as there is probably no competition between them and PAβN. Therefore, the presence of PAβN has no effect on the susceptibility to these antibiotics. In contrast, as LEV prefers to bind to the distal binding site with a good affinity, it could compete with PAβN for the distal binding pocket. Therefore, the presence of PAβN could decrease the amount of efflux of LEV by occupying the distal binding site. This potentially explains why PAβN could increase the susceptibility of certain antibiotics like LEV[57] and not others like GEN, CIP, and CHL.

2.2. Critical Interactions. GOLD molecular docking of PAβN to the binding site, located by Smina, also showed that the affinity of PAβN to the AdeB transporter (ΔG −42.9 kcal/mol and score 35.36) is favorable. Phe-cluster residues, including Phe136, Phe178, Phe569, Phe612, Phe623, and Phe669, provided effective π interactions between the ligand and the transporter. These strong interactions resulted in a higher score and favorable docking energy.

The interactions between PAβN and the key residues of the multibinding site of the AdeB transporter can be seen in Table 1 and Figure 4. PAβN binds to the space under the Phe loop, toward the Phe-cluster region that partly overlaps the distal binding site. PAβN is sandwiched between the Phe612 and Ser134 loops (Figure 4a). Additionally, the side chains containing residues Gln42 in the PN1 subdomain and the side chain containing residue Glu665 in the PC2 subdomain surround the guanidinium moiety of PAβN, and Met570 and Phe612 interact hydrophobically with the phenyl and naphthyl rings of PAβN, respectively. Ser134, Glu665, Thr668, and Gln42 form hydrogen bonds with PAβN (Table 1).

Detection of PAβN into the narrow channel (under the Phe loop) in AdeB suggests that the path under the Phe loop is wide enough for PAβN to pass through the transporter (Figure 4b).

2.3. Interaction Energies of the Phe Residues of the Distal Binding Site with PAβN. The analysis of the interaction energies between the residues of the binding site and PAβN in the complex shows the importance of the Phe residues in the interaction of PAβN with the transporter (Table 2). These results show a good series of interaction energies between PAβN and the Phe residues. More negative values in Table 2 represent the Phe residues that provided key interactions with PAβN at that time of the simulation. The tightest-interaction energy extracted from different snapshots of MD trajectories belongs to Phe612, during the 50 ns simulation. Table S2 series represent all of the interaction energies between the ligand and the key residues of the protein over the course of the MD simulation in which Phe and non-Phe residues are involved. However, the Phe residues form a hydrophobic microenvironment surrounding the ligand and make the area of the distal site suitable for strong hydrophobic interactions with ligands like PAβN and thereby prevent their efflux.

The high interaction energies between the Phe residues and PAβN during the MD simulation trajectories suggest the ordered switching of PAβN to different Phe residues to pass through the narrow channel and then the distal binding pocket, going toward the tunnel. PAβN appeared to behave like a climber as we observed switching of the interaction energies between the ligand and the key Phe residues of binding site during the course of the simulation. It used the Phe residues of the Phe-cluster as hooks to go forward in the channel. It appeared to climb and move upward in the distal binding pocket along the intramolecular channel of the transporter. The more favorable energies (Table 2) belonged to Phe612, located in the front, and Phe669, located behind PAβN (Figure 5). This indicates that the ligand had attraction to both sides simultaneously, which aided the forward movement by creating a hydrophobic trap.

To provide further information and to explore the role of the identified residues in ligand binding, we have carried out an in silico mutagenesis study. Blind molecular docking was performed to compare the affinity of PAβN to that of the mutated targets over the native form. The PAβn affinity of −9.6 kcal/mol to the native distal binding pocket of AdeB decreased for single mutant targets of F612G, F669G, and S134G to −8.4, −8.5, and 7.7 kcal/mol, respectively. The affinity after double mutation decreased to −8.0 kcal/mol for F612G−S134G, and surprisingly no pose in the distal binding pocket was observed

DOI: 10.1021/acsomega.7b00131
ACS Omega 2017, 2, 3002−3016

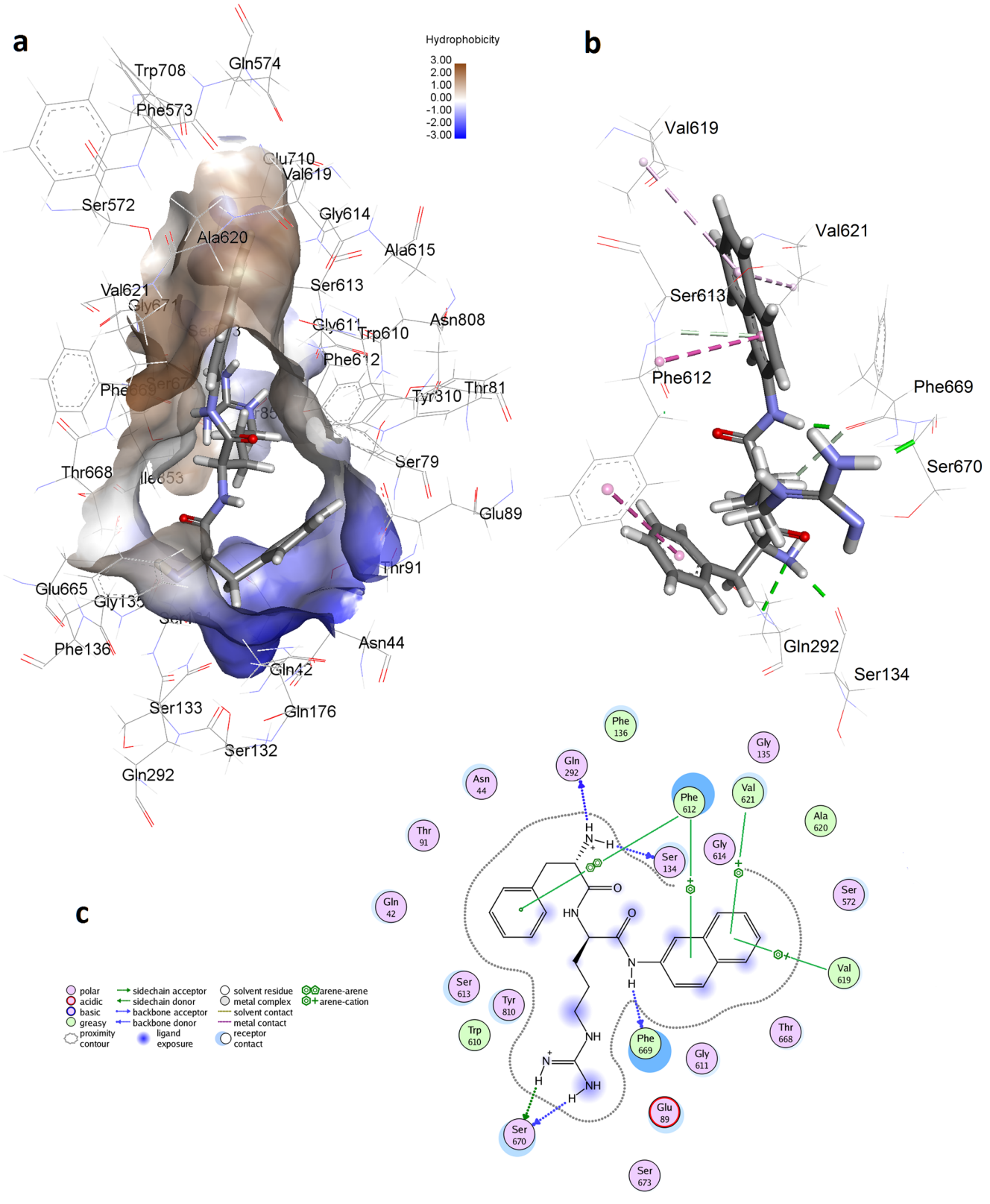

Figure 5. (a) Three-dimensional (3D) structure of PAβN in the binding monomer of *A. baumannii* AdeB. The average structure was calculated from the MD trajectories with surface format; the blue color represents low hydrophobicity (the side of the proximal binding site), and the brown areas represent the highly hydrophobic (the side of the distal binding pocket) region. (b) Three-dimensional structures of PAβN involved in the interaction with the binding monomer of AdeB. H-bonds are shown by the dotted green line and hydrophobic interactions by dotted pink lines. (c) Two-dimensional structure of PAβN in AdeB's binding site; the average structure of the complex (the figures were generated using the Accelrys discovery studio).

DOI: 10.1021/acsomega.7b00131
ACS Omega 2017, 2, 3002−3016

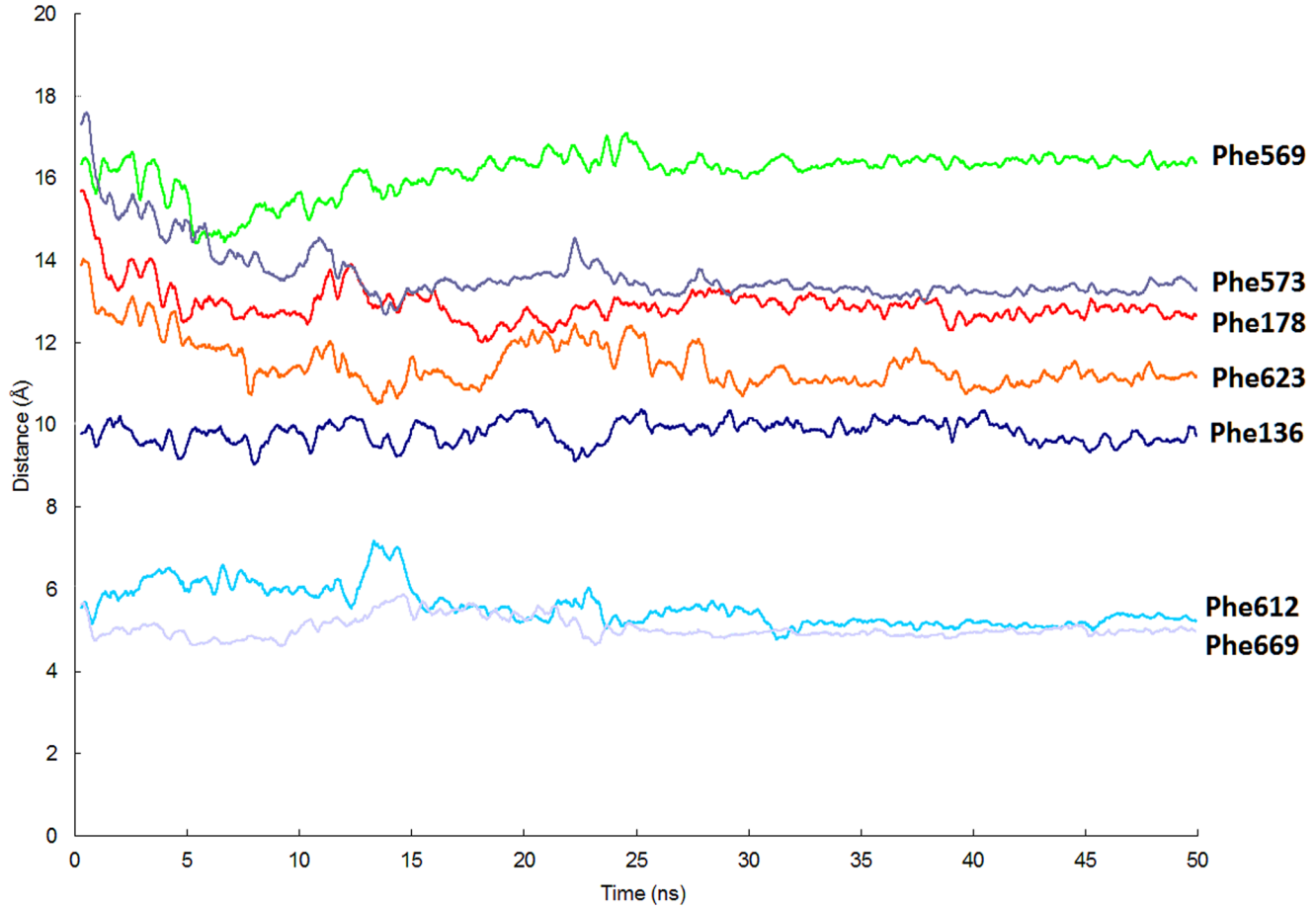

Figure 6. Distances between PAβN (atom N2) and residues of Phe-cluster (atom CG in the benzene ring of each Phe residue) in the multibinding site of the transporter.

for F612G−F669G. This in silico mutagenesis study further supports the importance of the identified residues in ligand binding. The distances between PAβN and each of the Phe residues that are close to the binding site were monitored during the 50 ns MD simulation of the complex (Figure 6). The distance between PAβN and the residue at the tip of the Phe loop in AdeB (Phe612) gradually decreased during the course of the simulation. It can be seen from Figure 6 that the trend of distances between Phe residues and PAβN during the course of MD simulation does not vary considerably, implying that the ligand faces considerable hindrance when passing through the Phe residues and the binding site, thus making its extrusion difficult.

Figure 7 shows the orientation of PAβN at the beginning, middle, and at the end of the MD simulations in the multisite pockets of the AdeB transporter. The Ser loop of the PN1 domain is on the other side of the narrow channel, under the Phe loop of PC1. The distance between Phe612 and Ser134 plays a critical role in modulating the size of channel's width, consequentially switching the ligand-accessible conformers of the binding protomer. This improved access allowed PAβN to bind to the binding site.

Figure S3a shows the changes in the width of the channel during the 50 ns MD simulation by monitoring the distance between Phe612 and Ser134. The channel width remains between 10 and 14 Å, which is wide enough for PAβN to pass through, as a small-molecular-mass ligand, during the course of the simulation.

2.4. Hydrogen Bond Analysis. The analysis of hydrogen bonds formed between the ligand and protein in the 50 ns MD trajectory showed just a few nonpermanent H-bond interactions (Table 3). Because the occupancy of these hydrogen bonds is relatively low (Table 3) during the simulation, the hydrogen-bonding interactions are unlikely to play dominant roles in the association of PAβN with the transporter. On the other hand, the hydrophobic interactions involving the Phe residues and PAβN remained strong during the course of MD simulation and most likely played a more significant role.

The fluctuation of the distance between a residue (Gln292) and the ligand during the MD simulation can be seen in FigureS2b. Although Gln292 has a potential to form hydrogen bond with PAβN, the distance between them in the first 30 ns was often more than 3.5 Å. This indicates that the hydrogen bond that may form is relatively short-lived and is unlikely to play an important role in the association between PAβN and the transporter.

2.5. Hydrophobic Microenvironment. The microenvironment of the binding site, surrounded by the nonpolar Phe residues and polar residues such as GLu89, Ser134, Ser670, Gln42, and Gln292, is shown in Figure 5c. Nonpolar residues provide a hydrophobic trap around PAβN in AdeB. Particularly, Phe residues that are in close contact with the ligand are important participants of the hydrophobic microenvironment. The hydrophobic microenvironment can also potentially help in strengthening the electrostatic interactions[58,59] between the ligand and the binding site residues (Figure 5a,b). This

DOI: 10.1021/acsomega.7b00131
ACS Omega 2017, 2, 3002−3016

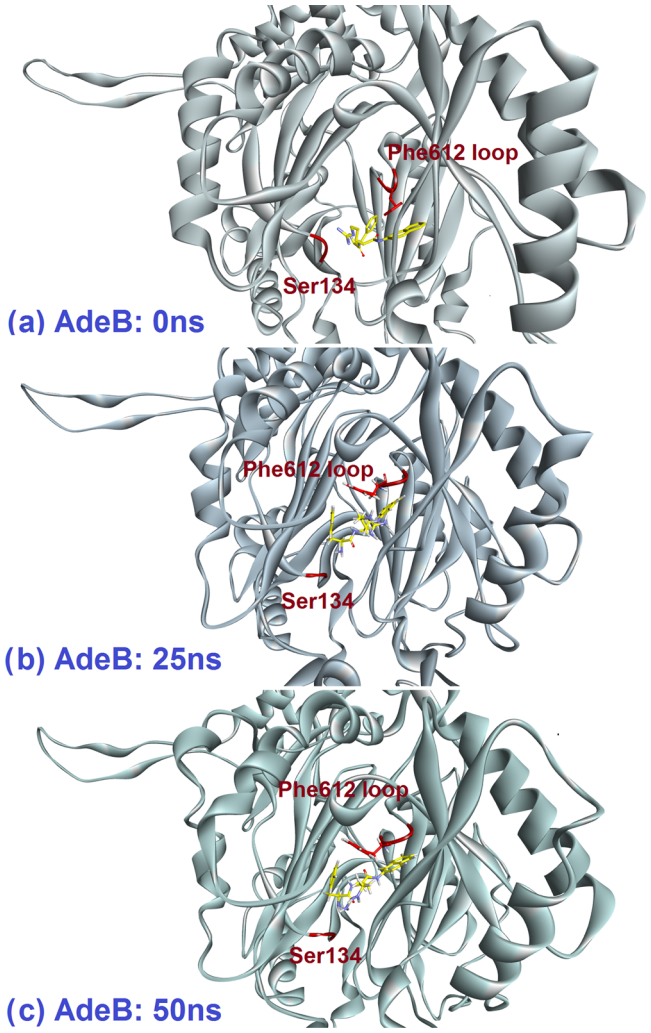

Figure 7. Structural snapshots at 0, 25, and 50 ns of the MD simulation showing the different orientations of PAβN within multibinding sites of the AdeB transporter and conformational changes of the Phe loop and Ser loop in the multibinding sites.

observation is the key to understanding the inhibition of the AdeB transporter by PAβN as this strong interaction traps the ligand in the binding pocket and consequently prevents the conformational switch.

The number and location of the Phe residues around the ligand were pivotal in creating a hydrophobic microenvironment, and the residues of the binding site of AdeB mostly interacted with PAβN through the formation of hydrophobic interactions, as seen in Figure 5b. Moreover, although some H-bonds can be observed, they do not appear to play any significant role due to their relatively short life time during the course of the simulation. The interactions between the key residues of the binding site of the AdeB transporter and PAβN after the 50 ns simulation can be seen in Table 4. The phenylalanine and β-naphthylamide groups of PAβN are involved in π interactions with Phe residues in the more hydrophobic part of the binding pocket, and the arginine residue of PAβN is involved in forming H-bonds with some residues such as Ser134, Gln42, Gln292, and Thr668 of the less hydrophobic part of the binding site.

2.6. Binding Free Energy. A total of 20 snapshots were collected from the last 200 ps of the MD simulation of the complex, and the binding free energy was calculated using the molecular mechanics, Poisson−Boltzmann surface area/molecular mechanics, generalized Born surface area (MM-PBSA/MM-GBSA) method.

The ΔG_{PB} value of −24.29 kcal/mol, obtained by MM-PBSA/MM-GBSA calculations, showed that the PAβN−AdeB complex is favorable (Table 5). In the binding free energy calculation, because normal mode analysis for calculating the entropy contribution is a time-consuming exercise even with good supercomputers, the value of 20 kcal/mol was considered for the contribution of the $-T\Delta S$ term in ligand binding, which has been used in the literature for similar ligands.[60] This provides a standard binding free energy (ΔG_{bind}) of −4.54 kcal/mol. The final estimated binding free energy (ΔG_{GB}) value of −34.06 kcal/mol further confirms that the complex between the ligand and the transporter is favorable.

The dissociation constant (K_d) for PAβN was obtained using the calculated total binding free energy using formula $\Delta G = RT \ln K_d$. Because the total binding free energy is directly proportional to the K_d value and inversely proportional to the binding affinity, the calculated value of 4.9×10^{-6} M for K_d suggests that PAβN binds to the transporter with a high affinity and acts as an inhibitor for the AdeB transporter.

2.7. Movement of PAβN across the Enter and Exit Tunnels. The analysis of the PAβN−transporter complex after the MD simulation using the MOLE 2.13.9.6 toolkit showed the possible entrance tunnels from the vestibule, from the lower external depression, and from the central cavity and also one exit port (Figure 8a). The exit port has access to the central cavity, the space between the three monomers of the transporter in the middle of the homotrimer structure, and the entrance ports have access to the periplasm or cytoplasm. The general entrance and exit points for the AdeB efflux pump transporter share structural similarity with the tunnels identified in *P. aeruginosa* AcrB and MexB by Nakashima et al.[8,61]

The key residues that are located in the gates of the tunnel are Leu666, Ser462, and Ser670 (Figure 8b). These amino acids play an important role in the movement of PAβN across the channel. Leu666 is located at the junction of channels 1 and 2, whereas Ser462 is halfway along channel 1 in the transporter and Ser670 of AdeB is located at the entrance of channel 2. The channels are between 1.35 and 3.85 Å wide, and this should allow PAβN to enter into the channels and move toward the exit port.

AdeB has two spacious multisite drug-binding pockets that line the drug translocation channel. PAβN, which is taken up

Table 3. Hydrogen Bonds Formed between PAβN and the Transporter during the 50 ns MD Simulation[a]

acceptor (res/atom)	donor (res/atom)	occupancy (%)	distance (Å)	angle (deg)
Gln292/NE2	PAβN/N	42.46	3.195 (0.19)	125.85 (22.09)
Glu665/OE2	PAβN/N4	19.38	2.940 (0.18)	68.35 (49.84)
PAβN/O1	Thr668/OG1	22.33	2.938 (0.22)	31.79 (20.40)

[a]Distance cutoff was set at 3.5 Å. Standard deviations are shown in parentheses.

DOI: 10.1021/acsomega.7b00131
ACS Omega 2017, 2, 3002−3016

Table 4. Different Kinds of Interactions between AdeB's Key Residues and PAβN after the 50 ns MD Simulation[a]

AdeB–PAβN atoms		distance	category	types
GLN292/HE21	PAβN/N	2.38872	hydrogen bond	conventional hydrogen bond
PAβN/N/H	SER134/O	2.06319	hydrogen bond	conventional hydrogen bond
PAβN/N2/H	PHE669/O	1.81724	hydrogen bond	conventional hydrogen bond
PAβN/N4/H	GLN42/OE1	2.27647	hydrogen bond	conventional hydrogen bond
PHE612/HN	PAβN	2.32546	hydrogen bond	π-donor hydrogen bond
PHE612	PAβN	5.56607	hydrophobic	π–π T-shaped
PAβN	VAL621	5.4717	hydrophobic	π-alkyl
PAβN	VAL619	4.63171	hydrophobic	π-alkyl
PAβN	VAL621	4.46385	hydrophobic	π-alkyl

[a]The distance cutoff and neighbor distance criterion were set to 5 and 4 Å, respectively. Proton donor–acceptor distances were considered for the H-bonds.

Table 5. Average Energy Contributions To Form the AdeB–PAβN Complex (kcal/mol) and Inhibition Constants ($K_{i/m}$ in Molar) with Standard Errors of the Mean (in Parentheses)

complex[c]	*A. baumannii* AdeB–PAβN
ΔE_{ele}	−30.36 (3.95)
ΔE_{vdw}	−55.42 (1.99)
ΔE_{int}	0.00
$\Delta E_{GAS(MM)}$	−85.78 (4.43)
ΔE_{PBsur}	−8.09 (0.66)
ΔE_{PBcal}	69.58 (4.34)
ΔE_{PBsol}	61.49 (4.55)
ΔE_{PBele}	39.21 (4.38)
ΔG_{PB}	−24.29 (3.94)
ΔE_{GBsur}	−8.09 (0.66)
ΔE_{GBcal}	59.81 (3.23)
ΔE_{GBsol}	51.73 (3.44)
ΔE_{GBele}	29.45 (3.06)
ΔG_{GB}	−34.06 (3.40)
$-T\Delta S$[a]	20
ΔG_{bind}	−4.54
K_d[b]	4.9×10^{-6}

[a]Estimated value based on the published results for similar-sized ligands.[60] [b]K_d is calculated through formula $\Delta G = RT \ln K_d$ using the values of binding energies resulted from analyzing simulations. [c]ΔE_{ELE} = electrostatic energy as calculated by the MM force field; ΔE_{vdw} = van der Waals contribution from MM; ΔE_{INT} = internal energy arising from the bond, angle, and dihedral terms in the MM force field (this term always amounts to 0 in the single trajectory approach); $\Delta E_{GAS(MM)}$ = total gas-phase energy (sum of ELE, vdw, and INT); $\Delta E_{PBSUR}/\Delta E_{GBSUR}$ = nonpolar contribution to the solvation free energy calculated by an empirical model; $\Delta E_{PBCAL}/\Delta E_{GBCAL}$ = the electrostatic contribution to the solvation free energy calculated by PB or GB, respectively; $\Delta E_{PBSOL}/\Delta E_{GBSOL}$ = sum of nonpolar and polar contributions to solvation; $\Delta E_{PBELE}/\Delta E_{GBELE}$ = sum of the electrostatic solvation free energy and MM electrostatic energy; $\Delta G_{PB}/\Delta G_{GB}$ = final estimated binding free energy calculated from the terms above (kcal/mol).

from the three possible entrances, could be transported by a peristaltic mechanism[62] through both pockets and can be potentially extruded from the top exit. The average structure obtained after the 50 ns MD simulation for the complex (Figure S4a) suggest that PAβN can enter into the binding monomer in the AdeB transporter with relative ease. Therefore, PAβN might act as a substrate for the AdeB transporter. In addition, according to the radius profile of the tunnels for entering and exporting of PAβN detected in the transporter (Figure S4b,c), the tunnels form internal pores that are wide enough to allow PAβN to pass through. Also Figure S5 depicts the view of the entrance and exit gates of PAβN in the AdeB transporter from the outside, which suggests that it may be possible to extrude PAβN from the transporter. However, because of the strong hydrophobic interaction with the Phe residues located within the binding pocket, it is likely that PAβN would remain trapped within the Phe-cluster and could not be extruded by the transporter.

2.8. Fluctuations and Flexibility of Binding Monomer Residues. According to the literature on the binding monomer, the Phe loop swings toward the ligand-binding site and, as a result, prevents ligands from binding to the proximal pocket in the binding monomer of AcrB and glycine residues in the Phe loop have a critical role in loop translocation.[8] In this study, the fluctuation of the residues in the ligand-free transporter and AdeB transporter in complex with PAβN during the course of MD simulation showed a considerably different root-mean-square fluctuation for Phe612 of AdeB in complex with PAβN in comparison to that in the ligand-free form of AdeB (Figure 9), which confirms the swing motion of the Phe loop. Additionally, an essential dynamics analysis has been performed (Figure S6), which further validates the swing motion of the Phe loop.

Binding monomer's residues in the complex exhibited a slightly more flexibility just for 50% of residues than that of the ligand-free form of the transporter in the structural alignment analysis (Figure 9). However, the key residues involved in the interaction with PAβN (e.g., Phe612, Phe136, Phe623, Phe669, and Phe672) showed notably less flexibility compared to that of the other residues of the binding monomer. This suggests that the presence of PAβN may have provided additional stability to the binding monomer. This can potentially prevent the switching of binding monomers to different conformations that are required to extrude a ligand by the transporter. This additional stability can be explained by the architecture of the binding site and its building blocks, particularly Phe building blocks. The presence of the Phe residues in the distal binding site creates a hydrophobic pocket. The energy calculation provides evidence that the Phe residues of the binding monomer in the form of Phe-clusters favorably interact with PAβN and trap the ligand in the distal pocket. This ultimately leads to the inhibition of the peristaltic mechanism and prevents the exporter from extruding any other substrates, leading to the inhibition of the tripartite pump. This observation is similar to that observed by Vargiu and Nikaido[7] for the PAβN interaction with the AcrB multibinding site. The movement of PAβN in the AcrB multibinding site caused it to straddle the G-loop (Phe617 loop) structure, which contributed

DOI: 10.1021/acsomega.7b00131
ACS Omega 2017, 2, 3002–3016

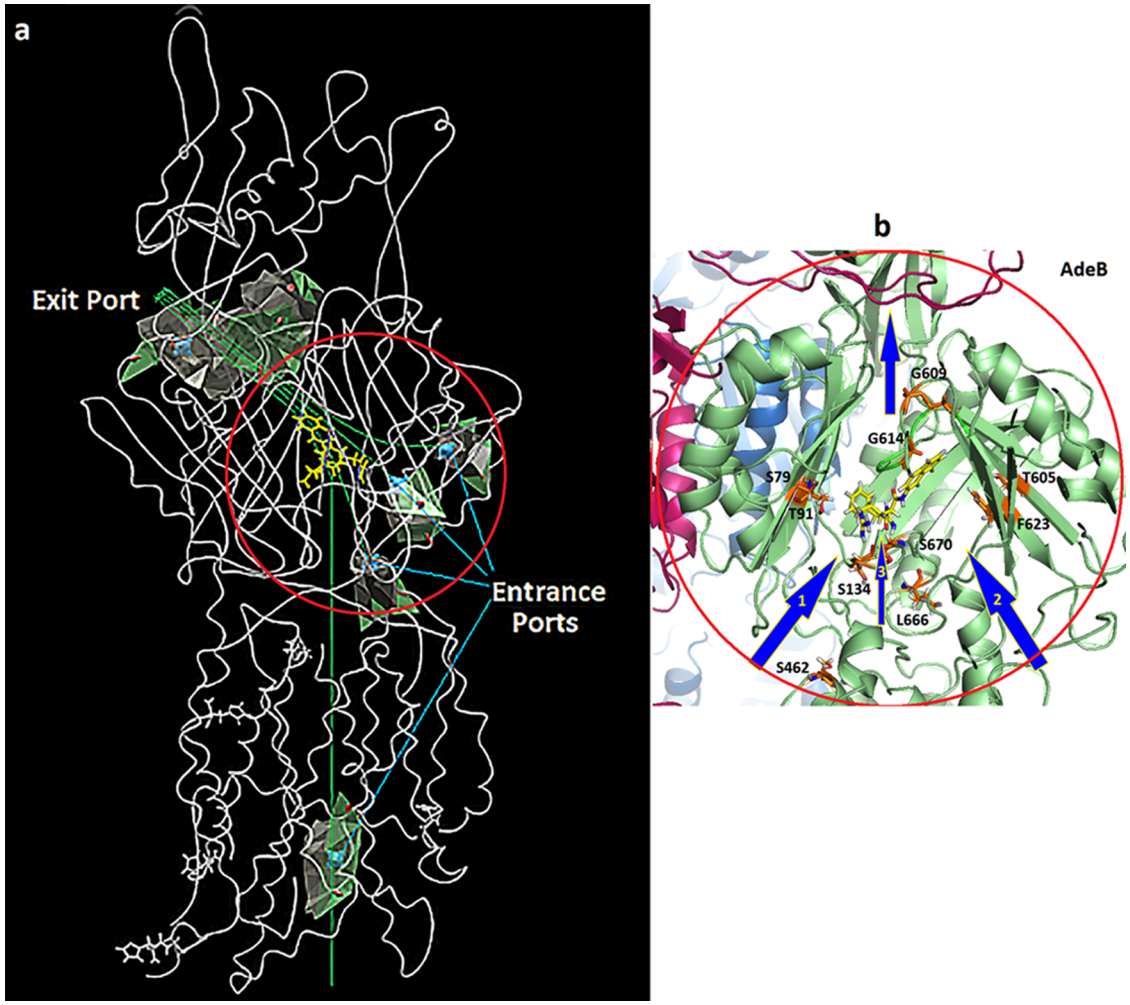

Figure 8. (a) General pattern for the entrance and exit ports in the binding monomer of the AdeB transporter (PAβN is in yellow color). (b) Zoomed-in view of the red circled area in (a) that shows the different entrance and exit tunnels in the AdeB transporter. The key residues located in the gates of tunnels and borders of the multisite binding pockets have been labeled. The green lines show the path of the travel of substrates through the pump.

to its ability to form interactions with the Phe residues. Recently, Kinana and co-workers[27] suggested that PAβN inhibits the efflux of other drugs by binding to the hydrophobic trap in the distal binding pocket of AcrB and interfering with the binding of other drug substrates to the upper part of the binding pocket. Our results for the AdeB transporter, in good agreement with the recent study, showed that PAβN does not considerably move inside AdeB and has a consistently strong interaction with Phe612 and other Phe residues of the distal binding pocket. The interaction of PAβN with the hydrophobic trap reduces the flexibility of the transporter, and this partly explains some of the inhibition mechanisms of PAβN. The study provides new information about the dual nature, a substrate and an inhibitor, of PAβN in its interaction with AdeB and partially explains the contradictory nature of the experimental data available in the literature.

It is urgent to develop specific inhibitors of efflux pumps to suppress the activities of these pumps and restore the sensitivity of bacteria, such as *A. baumannii*, to commonly used antibiotics to reverse antimicrobial resistance. Understanding the way in which the AdeB transporters identify and transport agents will help researchers to develop new strategies to tackle efflux-mediated resistance[63] and may provide inhibitors that will improve the efficacy of current antibiotics that are used to treat MDR infections in the clinic.[61] Development of molecular models of these tripartite pumps and their interaction with EPIs also pave the way to study a large number of potential leadlike molecules to develop potential inhibitors of these pumps.

3. CONCLUSIONS

Information obtained from this study provides detailed insight into the interaction of PAβN with the AdeB transporter in *A. baumannii*. The amino acid sequences in the binding site of the pump dictate the way in which PAβN interacts and either inhibits the transporter by interacting with the hydrophobic microenvironment with diverse strengths in the binding site of the complex or gets effluxed through the tunnel. It appeared from this study that the location and number of Phe residues, in the binding site, played a crucial role in stabilizing the PAβN–AdeB complex and kept the binding monomer in the binding stage. This could prevent the conformational switch of the binding monomer to access stage, which is essential to continue the peristaltic mechanism of the tripartite pump. We hope that the passage of PAβN through the transporter, the structure of the hydrophobic trap described in this study, and identification of the key residues of AdeB that interact with PAβN during the

DOI: 10.1021/acsomega.7b00131
ACS Omega 2017, 2, 3002–3016

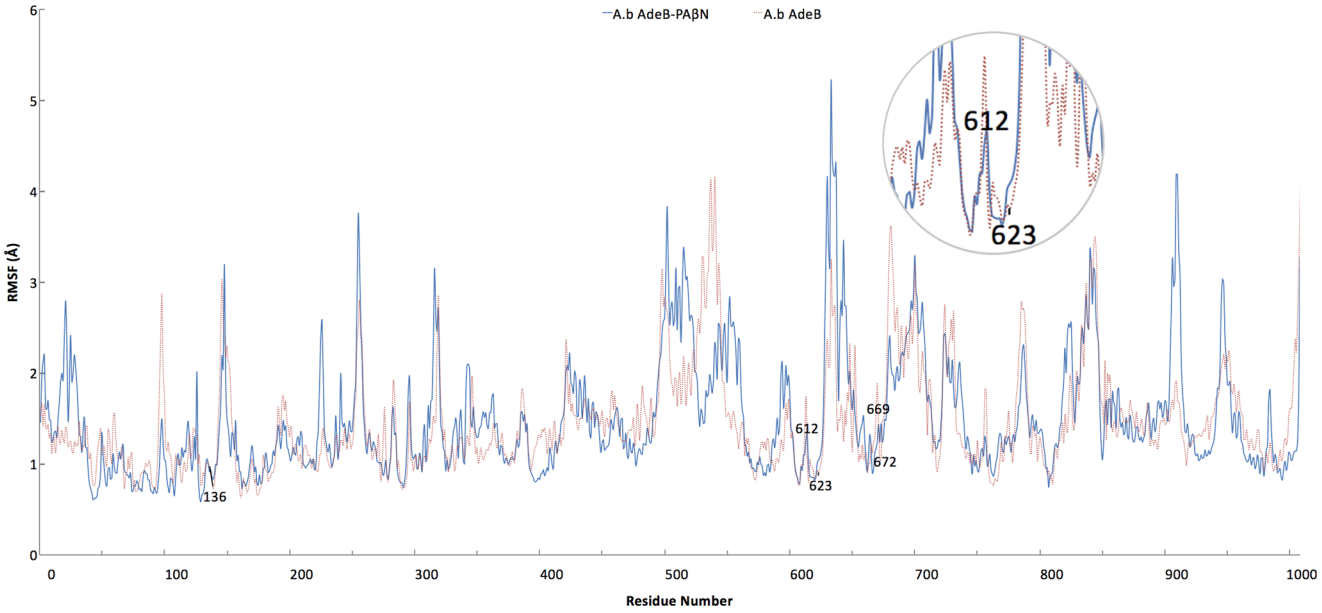

Figure 9. Atomic positional fluctuations (Å) of Cα atoms in the ligand-bound transporter (blue line) compared to those in the ligand-free protein (red line) in *A. baumannii* AdeB. The key residues, Phe612, Phe136, Phe623, Phe669, and Phe672, show notably less flexibility compared to that of the other residues.

simulation could contribute to the design of new effective and selective EPIs that may play key roles in reversing antimicrobial resistance.

4. COMPUTATIONAL METHODS

We explored the interaction of PAβN with the AdeB efflux pump transporter of *A. baumannii* using different computational methods, including MD simulation, MM-PBSA/MM-GBSA calculation, and molecular docking. Homology modeling was applied for the generation of the structural model of the homotrimer transporter in a PDB format.

4.1. Homology Modeling. The Swiss-Model web-server[64−68] was used for the homology modeling of the AdeB structural model using the FASTA formatted target sequence with UniProt entry number of B7I7F7_ACIB5, represented at the end of the Supporting Information. The crystal structure of AcrB from *E. coli* (PDB ID 1IWG) was selected as a template with a sequence identity of 50.36% in the amino acid sequence of the target. A comparison between the critical residues of the developed AdeB model and the template AcrB model is shown in Table S1.

The trimer of the AdeB protein was obtained as the final model from homology modeling in a 3D PDB structure format. The template that we used for the homology modeling was a monomer structure; therefore, the generated model was also a monomer structure and the assembly procedure was performed using the Accelrys discovery studio.[69] The generated model was without any gap, and all of the segments were solved. Accelrys discovery studio 4.5 was used to add probable missing side chains in the generated model. However, to eliminate the possibilities of steric clashes and suboptimal geometries, the structure was successfully minimized by the AMBER package program[70,71] before carrying out the MD simulations. The minimization was performed in vacuum through 1500 cycles, wherein 500 cycles of steepest descent were followed by 1000 cycles of conjugate gradient minimization. Figure S7 shows the validation of the structural model for the AdeB model, including the residue-wise profile, using ProSA analysis (protein structure analysis).[72,73] The *Z*-score of the model was within the range of scores calculated for proteins of similar size with experimentally determined structures, indicating good overall quality of the built model. The local similarity of AdeB monomers to the template target is shown in Figure S8.

4.2. Molecular Docking. Molecular docking protocols are methods that predict the preferred orientation of a bound ligand to a target that forms a stable complex. Knowledge of the preferred orientation in turn may be used to predict the strength of association between two molecules. For example, molecular docking has been performed to generate several distinct binding orientations and binding affinity for each binding mode. Subsequently, the lowest binding free energy has been considered as the most favorable binding mode for the system.

AutoDock Smina,[74] which uses the AutoDock Vina scoring function by default, was used for the blind molecular docking of PAβN to the AdeB structure for finding the best binding site in the homotrimer by exploring all probable binding cavities of the proteins. Smina was performed with default settings, which samples nine ligand conformations using the Vina docking routine of stochastic sampling. Then, GOLD molecular docking[75,76] was applied for the docking of PAβN to the Smina-located best binding site of the homotrimer for performing flexible molecular docking. On the basis of the fitness function scores and ligand-binding positions, the best-docked poses for the PAβN were selected. The lower fitness function score of the poses, generated using the GOLD program that has the highest GOLD fitness energy, reveals the best-docked pose.

The GOLD molecular docking procedure was performed by applying the GOLD protocol[76] in Accelrys discovery studio software. The genetic algorithm (GA) was used in GOLD ligand docking software to examine thoroughly the ligand conformational flexibility along with the partial flexibility of the protein.[77] The maximum number of runs for the ligand was set to 20, and in each run, a population size of 100 with 100 000 operations was employed. The number of islands was 5, and the

DOI: 10.1021/acsomega.7b00131
ACS Omega 2017, 2, 3002−3016

niche size of 2 was considered. The default cutoff value for hydrogen bonds was set to 2.5 Å (dH-X), and for the van der Waals distance, it was 4.0 Å. The GA docking was terminated when the top solutions attained the root-mean-square deviation (RMSD) values within 1.5 Å.[78]

4.3. MD Simulation. In this study, three MD simulation runs have been performed. The systems consisted of free PAβN, ligand-free protein of the *A. baumannii* AdeB homotrimer transporter, and a complex of PAβN−transporter that was obtained by GOLD molecular docking.

After the molecular docking, three 50 ns independent MD simulations were performed for the complex, ligand-free protein, and free ligand, which were followed by MM-PBSA/MM-GBSA calculations. All of the MD simulations were carried out using the AMBER 12.0 package. Each system was solvated using an octahedral box of TIP3P water molecules with a size of 174.81 × 153.69 × 229.20. Periodic boundary conditions and the particle-mesh Ewald method were employed in the simulations.[79] Particle-mesh Ewald method enabled us to calculate the "infinite" electrostatics without truncating the parameters. During each simulation, all bonds in which the hydrogen atom was present were considered fixed and all other bonds were constrained to their equilibrium values by applying the SHAKE algorithm.[80] The force field parameters for the ligand were generated using the ANTECHAMBER module of the AMBER program.

A cutoff radius of noncovalent interactions was set to 12 Å for the protein and complex, whereas for the free ligand simulations, the cutoff radius was set to 10 Å. Each minimization and equilibration phase was performed in two stages. In the first stage, ions and all water molecules were minimized for 500 cycles of steepest descent followed by 500 cycles of conjugate gradient minimization. Afterward, the whole system was minimized for a total of 2500 cycles without a restraint, wherein 1000 cycles of steepest descent were followed by 1500 cycles of conjugate gradient minimization. In the second stage, the systems were equilibrated for 500 ps, whereas the temperature was raised from 0 to 300 K. Then, equilibration was performed without a restraint for 100 ps, whereas the temperature was kept at 300 K. Sampling of reasonable configurations was conducted by running a 50 ns simulation with a 2 fs time step at 300 K and 1 atm pressure. A constant temperature was maintained by applying the Langevin algorithm, whereas the pressure was controlled by the isotropic position scaling protocol used in AMBER.[81] Time dependence of RMSD (Å) for the backbone atoms relative to the starting structure during 50 ns MD simulations of both ligand-free and ligand-bound AdeB is shown in Figure S9. RMSD curves show that both simulations have reached equilibrium after ∼30 ns, indicated by the relatively stable RMSD values from 30 ns to the end of the simulations.

4.4. MM-PBSA/MM-GBSA Calculations. Twenty snapshots were collected from the last 200 ps of simulations of the protein−ligand complex for post-processing analysis. The gas-phase interaction energy between the protein and the ligand, ΔE_{MM}, is the sum of electrostatic (ΔE_{ELE}), internal (ΔE_{INT}), and van der Waals (ΔE_{vdw}) interaction energies. The solvation free energy, ΔG_{sol}, is the sum of polar (ΔG_{PB}) and nonpolar (ΔG_{SA}) parts. The ΔG_{PB} term was calculated by solving the finite-difference Poisson−Boltzmann equation using the internal PBSA program.[71] The SCALE value was set to 5. The Parse radii were employed for all atoms.[82] The solvent probe radius was set at 1.4 Å (with the radii in the prmtop files). MM-PBSA running was performed with the PBSA module (PROC = 2). The value of the exterior dielectric constant was set at 80, and the solute dielectric constant was set at 1.[83] The nonpolar contribution was determined on the basis of the solvent-accessible surface area (SASA) using the LCPO method,[84] ΔG_{SA} = 0.04356 × ΔSASA, and CAVITY-OFFSET set at −1.008. Solute entropic contributions ($-T\Delta S$) were assumed to be +20 kcal/mol for the ligand in the complex.[60]

$$\Delta G_{bind} = \Delta G_{PB/GB} - T\Delta S$$

$$\Delta G_{PB/GB} = \Delta E_{GAS(MM)} + \Delta E_{PB/GBsol}$$

$$\Delta E_{GAS(MM)} = \Delta E_{internal} + \Delta E_{electrostatic} + \Delta E_{vdw}$$

$$\Delta E_{PB/GBsol} = \Delta E_{PB/GBsur} + \Delta E_{PB/GBcal}$$

In the MM-GBSA calculations, like the MM-PBSA calculations, the gas-phase interaction energy ($\Delta E_{GAS(MM)}$) and the nonpolar and polar ($\Delta E_{PB/GBsol}$) parts of the solvation energy were calculated. The electrostatic solvation energy (ΔG_{GB}) was calculated using GB models.[85] A value of 80 was used for the exterior dielectric constant, and a value of 1 was used for the solute dielectric constant. The binding free energies were calculated using both the MM-PBSA and MM-GBSA methods.

■ ASSOCIATED CONTENT

Supporting Information

The Supporting Information is available free of charge on the ACS Publications website at DOI: 10.1021/acsomega.7b00131.

Figures containing the protein sequence alignment, binding mode of the different ligands in the AdeB transporter, distances between the ligand and key residues, tunnels in the AdeB efflux pump, outside view of PAβN in the binding site of the AdeB transporter, essential dynamics analysis (PCA), the validation of the structural model superimposing the 3D structures of the template and target of time dependence of RMSD and tables showing the crucial regions in the AcrB and AdeB transporters, interaction energies between key residues, and PAβN and FASTA sequence of the AdeB transporter of *A. baumannii* (PDF)

■ AUTHOR INFORMATION

Corresponding Author

*E-mail: k.miraz.rahman@kcl.ac.uk. Tel: +44 (0)20 7848 1891.

ORCID

Khondaker Miraz Rahman: 0000-0001-8566-8648

Notes

The authors declare no competing financial interest.

■ ACKNOWLEDGMENTS

We gratefully acknowledge the support provided by the High-Performance Compute Cluster (HPC) of King's College London (Ada and Rosalind).

■ REFERENCES

(1) Magnet, S.; Courvalin, P.; Lambert, T. Resistance-nodulation-cell division-type efflux pump involved in aminoglycoside resistance in *Acinetobacter baumannii* strain BM4454. *Antimicrob. Agents Chemother.* **2001**, *45*, 3375−3380.

DOI: 10.1021/acsomega.7b00131
ACS Omega 2017, 2, 3002−3016

(2) Ruiz, N.; Kahne, D.; Silhavy, T. J. Transport of lipopolysaccharide across the cell envelope: the long road of discovery. *Nat. Rev. Microbiol.* **2009**, *7*, 677−683.
(3) Silhavy, T. J.; Kahne, D.; Walker, S. The bacterial cell envelope. *Cold Spring Harbor Perspect. Biol.* **2010**, *2*, No. a000414.
(4) Murakami, S.; Nakashima, R.; Yamashita, E.; Matsumoto, T.; Yamaguchi, A. Crystal structures of a multidrug transporter reveal a functionally rotating mechanism. *Nature* **2006**, *443*, 173−179.
(5) Murakami, S.; Nakashima, R.; Yamashita, E.; Yamaguchi, A. Crystal structure of bacterial multidrug efflux transporter AcrB. *Nature* **2002**, *419*, 587−593.
(6) Seeger, M. A.; Schiefner, A.; Eicher, T.; Verrey, F.; Diederichs, K.; Pos, K. M. Structural asymmetry of AcrB trimer suggests a peristaltic pump mechanism. *Science* **2006**, *313*, 1295−1298.
(7) Vargiu, A. V.; Nikaido, H. Multidrug binding properties of the AcrB efflux pump characterized by molecular dynamics simulations. *Proc. Natl. Acad. Sci. U.S.A.* **2012**, *109*, 20637−20642.
(8) Nakashima, R.; Sakurai, K.; Yamasaki, S.; Nishino, K.; Yamaguchi, A. Structures of the multidrug exporter AcrB reveal a proximal multisite drug-binding pocket. *Nature* **2011**, *480*, 565−569.
(9) Eicher, T.; Cha, H. J.; Seeger, M. A.; Brandstatter, L.; El-Delik, J.; Bohnert, J. A.; Kern, W. V.; Verrey, F.; Grutter, M. G.; Diederichs, K.; Pos, K. M. Transport of drugs by the multidrug transporter AcrB involves an access and a deep binding pocket that are separated by a switch-loop. *Proc. Natl. Acad. Sci. U.S.A.* **2012**, *109*, 5687−5692.
(10) Kobayashi, N.; Tamura, N.; van Veen, H. W.; Yamaguchi, A.; Murakami, S. beta-Lactam selectivity of multidrug transporters AcrB and AcrD resides in the proximal binding pocket. *J. Biol. Chem.* **2014**, *289*, 10680−10690.
(11) Sennhauser, G.; Bukowska, M. A.; Briand, C.; Grutter, M. G. Crystal structure of the multidrug exporter MexB from *Pseudomonas aeruginosa*. *J. Mol. Biol.* **2009**, *389*, 134−145.
(12) Dijkshoorn, L.; Nemec, A.; Seifert, H. An increasing threat in hospitals: multidrug-resistant *Acinetobacter baumannii*. *Nat. Rev. Microbiol.* **2007**, *5*, 939−951.
(13) Peleg, A. Y.; Seifert, H.; Paterson, D. L. *Acinetobacter baumannii*: emergence of a successful pathogen. *Clin. Microbiol. Rev.* **2008**, *21*, 538−582.
(14) Seeger, M. A.; von Ballmoos, C.; Eicher, T.; Brandstatter, L.; Verrey, F.; Diederichs, K.; Pos, K. M. Engineered disulfide bonds support the functional rotation mechanism of multidrug efflux pump AcrB. *Nat. Struct. Mol. Biol.* **2008**, *15*, 199−205.
(15) Yoon, E.-J.; Chabane, Y. N.; Goussard, S.; Snesrud, E.; Courvalin, P.; Dé, E.; Grillot-Courvalin, C. Contribution of resistance-nodulation-cell division efflux systems to antibiotic resistance and biofilm formation in *Acinetobacter baumannii*. *mBio* **2015**, *6*, No. e00309.
(16) Aires, J. R.; Nikaido, H. Aminoglycosides are captured from both periplasm and cytoplasm by the AcrD multidrug efflux transporter of *Escherichia coli*. *J. Bacteriol.* **2005**, *187*, 1923−1929.
(17) Eswaran, J.; Koronakis, E.; Higgins, M. K.; Hughes, C.; Koronakis, V. Three's company: component structures bring a closer view of tripartite drug efflux pumps. *Curr. Opin. Struct. Biol.* **2004**, *14*, 741−747.
(18) Paulsen, I. T. Multidrug efflux pumps and resistance: regulation and evolution. *Curr. Opin. Microbiol.* **2003**, *6*, 446−451.
(19) Wieczorek, P.; Sacha, P.; Hauschild, T.; Zorawski, M.; Krawczyk, M.; Tryniszewska, E. Multidrug resistant *Acinetobacter baumannii*–the role of AdeABC (RND family) efflux pump in resistance to antibiotics. *Folia Histochem. Cytobiol.* **2008**, *46*, 257−267.
(20) Marchand, I.; Damier-Piolle, L.; Courvalin, P.; Lambert, T. Expression of the RND-type efflux pump AdeABC in *Acinetobacter baumannii* is regulated by the AdeRS two-component system. *Antimicrob. Agents Chemother.* **2004**, *48*, 3298−3304.
(21) Fournier, P. E.; Vallenet, D.; Barbe, V.; Audic, S.; Ogata, H.; Poirel, L.; Richet, H.; Robert, C.; Mangenot, S.; Abergel, C.; Nordmann, P.; Weissenbach, J.; Raoult, D.; Claverie, J. M. Comparative genomics of multidrug resistance in *Acinetobacter baumannii*. *PLoS Genet.* **2006**, *2*, No. e7.
(22) Higgins, P. G.; Wisplinghoff, H.; Stefanik, D.; Seifert, H. Selection of topoisomerase mutations and overexpression of adeB mRNA transcripts during an outbreak of *Acinetobacter baumannii*. *J. Antimicrob. Chemother.* **2004**, *54*, 821−823.
(23) Vila, J.; Marti, S.; Sanchez-Cespedes, J. Porins, efflux pumps and multidrug resistance in *Acinetobacter baumannii*. *J. Antimicrob. Chemother.* **2007**, *59*, 1210−1215.
(24) Peleg, A. Y.; Adams, J.; Paterson, D. L. Tigecycline Efflux as a Mechanism for Nonsusceptibility in *Acinetobacter baumannii*. *Antimicrob. Agents Chemother.* **2007**, *51*, 2065−2069.
(25) Ruzin, A.; Keeney, D.; Bradford, P. A. AdeABC multidrug efflux pump is associated with decreased susceptibility to tigecycline in *Acinetobacter calcoaceticus-Acinetobacter baumannii* complex. *J. Antimicrob. Chemother.* **2007**, *59*, 1001−1004.
(26) Lomovskaya, O.; Warren, M. S.; Lee, A.; Galazzo, J.; Fronko, R.; Lee, M.; Blais, J.; Cho, D.; Chamberland, S.; Renau, T.; Leger, R.; Hecker, S.; Watkins, W.; Hoshino, K.; Ishida, H.; Lee, V. J. Identification and characterization of inhibitors of multidrug resistance efflux pumps in *Pseudomonas aeruginosa*: novel agents for combination therapy. *Antimicrob. Agents Chemother.* **2001**, *45*, 105−116.
(27) Kinana, A. D.; Vargiu, A. V.; May, T.; Nikaido, H. Aminoacyl beta-naphthylamides as substrates and modulators of AcrB multidrug efflux pump. *Proc. Natl. Acad. Sci. U.S.A.* **2016**, *113*, 1405−1410.
(28) Blanchard, C.; Barnett, P.; Perlmutter, J.; Dunman, P. M. Identification of *Acinetobacter baumannii* serum-associated antibiotic efflux pump inhibitors. *Antimicrob. Agents Chemother.* **2014**, *58*, 6360−6370.
(29) Rajamohan, G.; Srinivasan, V. B.; Gebreyes, W. A. Novel role of *Acinetobacter baumannii* RND efflux transporters in mediating decreased susceptibility to biocides. *J. Antimicrob. Chemother.* **2010**, *65*, 228−232.
(30) Chen, Y.; Pi, B.; Zhou, H.; Yu, Y.; Li, L. Triclosan resistance in clinical isolates of *Acinetobacter baumannii*. *J. Med. Microbiol.* **2009**, *58*, 1086−1091.
(31) Baucheron, S.; Imberechts, H.; Chaslus-Dancla, E.; Cloeckaert, A. The AcrB multidrug transporter plays a major role in high-level fluoroquinolone resistance in *Salmonella enterica serovar typhimurium* phage type DT204. *Microb Drug Resist* **2002**, *8*, 281−289.
(32) Mamelli, L.; Amoros, J. P.; Pages, J. M.; Bolla, J. M. A phenylalanine-arginine beta-naphthylamide sensitive multidrug efflux pump involved in intrinsic and acquired resistance of Campylobacter to macrolides. *Int. J. Antimicrob. Agents* **2003**, *22*, 237−241.
(33) Hasdemir, U. O.; Chevalier, J.; Nordmann, P.; Pages, J. M. Detection and prevalence of active drug efflux mechanism in various multidrug-resistant *Klebsiella pneumoniae* strains from Turkey. *J. Clin. Microbiol.* **2004**, *42*, 2701−2706.
(34) Chevalier, J.; Pages, J. M.; Eyraud, A.; Mallea, M. Membrane permeability modifications are involved in antibiotic resistance in *Klebsiella pneumoniae*. *Biochem. Biophys. Res. Commun.* **2000**, *274*, 496−499.
(35) Yoshida, K.; Nakayama, K.; Yokomizo, Y.; Ohtsuka, M.; Takemura, M.; Hoshino, K.; Kanda, H.; Namba, K.; Nitanai, H.; Zhang, J. Z.; Lee, V. J.; Watkins, W. J. MexAB-OprM specific efflux pump inhibitors in *Pseudomonas aeruginosa*. Part 6: exploration of aromatic substituents. *Bioorg. Med. Chem.* **2006**, *14*, 8506−8518.
(36) Lomovskaya, O.; Bostian, K. A. Practical applications and feasibility of efflux pump inhibitors in the clinic–a vision for applied use. *Biochem. Pharmacol.* **2006**, *71*, 910−918.
(37) Pagès, J. M.; Masi, M.; Barbe, J. Inhibitors of efflux pumps in Gram-negative bacteria. *Trends Mol. Med.* **2005**, *11*, 382−389.
(38) Mahamoud, A.; Chevalier, J.; Alibert-Franco, S.; Kern, W. V.; Pages, J. M. Antibiotic efflux pumps in Gram-negative bacteria: the inhibitor response strategy. *J. Antimicrob. Chemother.* **2007**, *59*, 1223−1229.
(39) Malléa, M.; Chevalier, J.; Eyraud, A.; Pages, J. M. Inhibitors of antibiotic efflux pump in resistant *Enterobacter aerogenes* strains. *Biochem. Biophys. Res. Commun.* **2002**, *293*, 1370−1373.
(40) Mazzariol, A.; Tokue, Y.; Kanegawa, T. M.; Cornaglia, G.; Nikaido, H. High-level fluoroquinolone-resistant clinical isolates of

DOI: 10.1021/acsomega.7b00131
ACS Omega 2017, 2, 3002−3016

Escherichia coli overproduce multidrug efflux protein AcrA. *Antimicrob. Agents Chemother.* **2000**, *44*, 3441−3443.
(41) Pannek, S.; Higgins, P. G.; Steinke, P.; Jonas, D.; Akova, M.; Bohnert, J. A.; Seifert, H.; Kern, W. V. Multidrug efflux inhibition in *Acinetobacter baumannii*: comparison between 1-(1-naphthylmethyl)-piperazine and phenyl-arginine-beta-naphthylamide. *J. Antimicrob. Chemother.* **2006**, *57*, 970−974.
(42) Cortez-Cordova, J.; Kumar, A. Activity of the efflux pump inhibitor phenylalanine-arginine beta-naphthylamide against the AdeFGH pump of *Acinetobacter baumannii*. *Int. J. Antimicrob. Agents* **2011**, *37*, 420−424.
(43) Hannula, M.; Hanninen, M. L. Effect of putative efflux pump inhibitors and inducers on the antimicrobial susceptibility of *Campylobacter jejuni* and *Campylobacter coli*. *J. Med. Microbiol.* **2008**, *57*, 851−855.
(44) Lin, J.; Martinez, A. Effect of efflux pump inhibitors on bile resistance and in vivo colonization of *Campylobacter jejuni*. *J. Antimicrob. Chemother.* **2006**, *58*, 966−972.
(45) Borges-Walmsley, M. I.; McKeegan, K. S.; Walmsley, A. R. Structure and function of efflux pumps that confer resistance to drugs. *Biochem. J.* **2003**, *376*, 313−338.
(46) Li, X. Z.; Nikaido, H. Efflux-mediated drug resistance in bacteria. *Drugs* **2004**, *64*, 159−204.
(47) Poole, K. Multidrug resistance in Gram-negative bacteria. *Curr. Opin. Microbiol.* **2001**, *4*, 500−508.
(48) Poole, K. Efflux-mediated antimicrobial resistance. *J. Antimicrob. Chemother.* **2005**, *56*, 20−51.
(49) Hooper, D. C. Efflux pumps and nosocomial antibiotic resistance: a primer for hospital epidemiologists. *Clin. Infect. Dis.* **2005**, *40*, 1811−1817.
(50) Piddock, L. J. Clinically relevant chromosomally encoded multidrug resistance efflux pumps in bacteria. *Clin. Microbiol. Rev.* **2006**, *19*, 382−402.
(51) Du, D.; van Veen, H. W.; Luisi, B. F. Assembly and operation of bacterial tripartite multidrug efflux pumps. *Trends Microbiol.* **2015**, *23*, 311−319.
(52) Richmond, G. E.; Evans, L. P.; Anderson, M. J.; Wand, M. E.; Bonney, L. C.; Ivens, A.; Chua, K. L.; Webber, M. A.; Sutton, J. M.; Peterson, M. L.; Piddock, L. J. The *Acinetobacter baumannii* Two-Component System AdeRS Regulates Genes Required for Multidrug Efflux, Biofilm Formation, and Virulence in a Strain-Specific Manner. *mBio* **2016**, *7*, No. e00430.
(53) Nowak, J.; Seifert, H.; Higgins, P. G. Prevalence of eight resistance-nodulation-division efflux pump genes in epidemiologically characterized *Acinetobacter baumannii* of worldwide origin. *J. Med. Microbiol.* **2015**, *64*, 630−635.
(54) Lin, M. F.; Lin, Y. Y.; Tu, C. C.; Lan, C. Y. Distribution of different efflux pump genes in clinical isolates of multidrug-resistant *Acinetobacter baumannii* and their correlation with antimicrobial resistance. *J. Microbiol., Immunol. Infect.* **2015**, *50*, 224−231.
(55) Wieczorek, P.; Sacha, P.; Czaban, S.; Hauschild, T.; Ojdana, D.; Kowalczuk, O.; Milewski, R.; Poniatowski, B.; Niklinski, J.; Tryniszewska, E. Distribution of AdeABC efflux system genes in genotypically diverse strains of clinical *Acinetobacter baumannii*. *Diagn Microbiol Infect Dis* **2013**, *77*, 106−109.
(56) Takatsuka, Y.; Chen, C.; Nikaido, H. Mechanism of recognition of compounds of diverse structures by the multidrug efflux pump AcrB of *Escherichia coli*. *Proc. Natl. Acad. Sci. U.S.A.* **2010**, *107*, 6559−6565.
(57) Lamers, R. P.; Cavallari, J. F.; Burrows, L. L. The efflux inhibitor phenylalanine-arginine beta-naphthylamide (PAbetaN) permeabilizes the outer membrane of gram-negative bacteria. *PLoS One* **2013**, *8*, No. e60666.
(58) Jamshidi, S.; Jalili, S.; Rafii-Tabar, H. Study of orotidine 5′-monophosphate decarboxylase in complex with the top three OMP, BMP, and PMP ligands by molecular dynamics simulation. *J. Biomol. Struct. Dyn.* **2015**, *33*, 404−417.
(59) Malabanan, M. M.; Amyes, T. L.; Richard, J. P. A role for flexible loops in enzyme catalysis. *Curr. Opin. Struct. Biol.* **2010**, *20*, 702−710.
(60) Chong, L. T.; Duan, Y.; Wang, L.; Massova, I.; Kollman, P. A. Molecular dynamics and free-energy calculations applied to affinity maturation in antibody. *Proc. Natl. Acad. Sci.* **1999**, *96*, 14330−14335.
(61) Nakashima, R.; Sakurai, K.; Yamasaki, S.; Hayashi, K.; Nagata, C.; Hoshino, K.; Onodera, Y.; Nishino, K.; Yamaguchi, A. Structural basis for the inhibition of bacterial multidrug exporters. *Nature* **2013**, *500*, 102−106.
(62) Pos, K. M. Drug transport mechanism of the AcrB efflux pump. *Biochim. Biophys. Acta* **2009**, *1794*, 782−793.
(63) Collu, F.; Vargiu, A. V.; Dreier, J.; Cascella, M.; Ruggerone, P. Recognition of imipenem and meropenem by the RND-transporter MexB studied by computer simulations. *J. Am. Chem. Soc.* **2012**, *134*, 19146−19158.
(64) Schwede, T.; Kopp, J.; Guex, N.; Peitsch, M. C. SWISS-MODEL: An automated protein homology-modeling server. *Nucleic Acids Res.* **2003**, *31*, 3381−3385.
(65) Arnold, K.; Bordoli, L.; Kopp, J.; Schwede, T. The SWISS-MODEL workspace: a web-based environment for protein structure homology modelling. *Bioinformatics* **2006**, *22*, 195−201.
(66) Guex, N.; Peitsch, M. C.; Schwede, T. Automated comparative protein structure modeling with SWISS-MODEL and Swiss-PdbViewer: a historical perspective. *Electrophoresis* **2009**, *30*, S162−S173.
(67) Kiefer, F.; Arnold, K.; Kunzli, M.; Bordoli, L.; Schwede, T. The SWISS-MODEL Repository and associated resources. *Nucleic Acids Res.* **2009**, *37*, D387−D392.
(68) Biasini, M.; Bienert, S.; Waterhouse, A.; Arnold, K.; Studer, G.; Schmidt, T.; Kiefer, F.; Gallo Cassarino, T.; Bertoni, M.; Bordoli, L.; Schwede, T. SWISS-MODEL: modelling protein tertiary and quaternary structure using evolutionary information. *Nucleic Acids Res.* **2014**, *42*, W252−W258.
(69) Biovia, D. S. *Discovery Studio Modeling Environment, release 4.5*; Dassault Systèmes: San Diego, 2015.
(70) Case, D. A.; Cheatham, T. E., 3rd; Darden, T.; Gohlke, H.; Luo, R.; Merz, K. M., Jr.; Onufriev, A.; Simmerling, C.; Wang, B.; Woods, R. J. The Amber biomolecular simulation programs. *J. Comput. Chem.* **2005**, *26*, 1668−1688.
(71) Case, D. A.; Darden, T. A.; Cheatham, T. E.; Simmerling, C. L.; Wang, J.; Duke, R. E.; Luo, R.; Walker, R. C.; Zhang, W.; Merz, K. M.; Roberts, B.; Hayik, S.; Roitberg, A.; Seabra, G.; Swails, J.; Götz, A. W.; Kolossváry, I.; Wong, K. F.; Paesani, F.; Vanicek, J.; Wolf, R. M.; Liu, J.; Wu, X.; Brozell, S. R.; Steinbrecher, T.; Gohlke, H.; Cai, Q.; Wang, X.; Ye, J.; Hsieh, M.-J.; Cui, G.; Roe, D. R.; Mathews, D. H.; Seetin, M. G.; Salomon-Ferrer, R.; Sagui, C.; Babin, V.; Luchko, T.; Gusarov, S.; Kovalenko, A.; Kollman, P. A. *AMBER 12*; University of California: San Francisco, 2012.
(72) Sippl, M. J. Recognition of errors in three-dimensional structures of proteins. *Proteins* **1993**, *17*, 355−362.
(73) Wiederstein, M.; Sippl, M. J. ProSA-web: interactive web service for the recognition of errors in three-dimensional structures of proteins. *Nucleic Acids Res.* **2007**, *35*, W407−W410.
(74) Koes, D. R.; Baumgartner, M. P.; Camacho, C. J. Lessons learned in empirical scoring with smina from the CSAR 2011 benchmarking exercise. *J. Chem. Inf. Model.* **2013**, *53*, 1893−1904.
(75) Jones, G.; Willett, P.; Glen, R. C. Molecular recognition of receptor sites using a genetic algorithm with a description of desolvation. *J. Mol. Biol.* **1995**, *245*, 43−53.
(76) Jones, G.; Willett, P.; Glen, R. C.; Leach, A. R.; Taylor, R. Development and validation of a genetic algorithm for flexible docking. *J. Mol. Biol.* **1997**, *267*, 727−748.
(77) Nissink, J. W.; Murray, C.; Hartshorn, M.; Verdonk, M. L.; Cole, J. C.; Taylor, R. A new test set for validating predictions of protein-ligand interaction. *Proteins* **2002**, *49*, 457−471.
(78) Jamshidi, S.; Rafii-Tabar, H.; Jalili, S. Investigation into mechanism of orotidine 5′-monophosphate decarboxylase enzyme by MM-PBSA/MM-GBSA and molecular docking. *Mol. Simul.* **2014**, *40*, 469−476.

DOI: 10.1021/acsomega.7b00131
ACS Omega 2017, 2, 3002−3016

(79) Darden, T.; York, D.; Pedersen, L. Particle Mesh Ewald - an N.Log(N) Method for Ewald Sums in Large Systems. *J. Chem. Phys.* **1993**, *98*, 10089.
(80) Ryckaert, J. P.; Ciccotti, G.; Berendsen, H. J. C. Numerical-Integration of Cartesian Equations of Motion of a System with Constraints - Molecular-Dynamics of N-Alkanes. *J. Comput. Phys.* **1977**, *23*, 327.
(81) Case, D. A.; Cheatham, T. E.; Darden, T.; Gohlke, H.; Luo, R.; Merz, K. M.; Onufriev, A.; Simmerling, C.; Wang, B.; Woods, R. J. The Amber biomolecular simulation programs. *J. Comput. Chem.* **2005**, *26*, 1668−1688.
(82) Sitkoff, D.; Sharp, K. A.; Honig, B. Accurate Calculation of Hydration Free-Energies Using Macroscopic Solvent Models. *J. Phys. Chem.* **1994**, *98*, 1978−1988.
(83) Wang, W.; Kollman, P. A. Free energy calculations on dimer stability of the HIV protease using molecular dynamics and a continuum solvent model. *J. Mol. Biol.* **2000**, *303*, 567.
(84) Weiser, J.; Shenkin, P. S.; Still, W. C. Approximate atomic surfaces from linear combinations of pairwise overlaps (LCPO). *J. Comput. Chem.* **1999**, *20*, 217−230.
(85) Tsui, V.; Case, D. A. Theory and applications of the generalized Born solvation model in macromolecular simulations. *Biopolymers* **2000**, *56*, 275−291.

DOI: 10.1021/acsomega.7b00131
ACS Omega 2017, 2, 3002−3016